Prabha Materials Science Letters
Vol. 3, No. 2, 242-253, 2024
https://doi.org/10.33889/PMSL.2024.3.2.015

Ram Arti Publishers

# Electromagnetic Interference Shielding Properties of $SrFe_{12-2x}(Cu_{0.5}Co_{0.5}Ti)_xO_{19}$ Hexaferrite

**Huynh Ngoc Toan**
Faculty of Natural Sciences and Institute of Research and Development,
Duy Tan University, Da Nang, Viet Nam.
E-mail: huynhngoctoan@duytan.edu.vn

**Chu Thi Anh Xuan**
Institute of Science and Technology,
TNU-University of Sciences, Thai Nguyen, Viet Nam.
E-mail: xuancta@tnus.edu.vn

**Nguyen Quy Tuan**
The University of Danang - University of Science and Education,
Da Nang, 550000, Viet Nam.
E-mail: nqtuan@ued.udn.vn

**Ngo Tran**
Institute of Research and Development and Faculty of Natural Sciences,
Duy Tan University, Da Nang, Viet Nam.
*Corresponding author*: tranngo@duytan.edu.vn

(Received on June 25, 2024; Revised on July 30, 2024; Accepted on July 31, 2024)

**Abstract**
Electromagnetic (EM) pollution has become one of the most severe forms of pollution for humans and electronic devices. In order to protect humans and electronic devices from electromagnetic interference (EMI), the material that could shield the EMI should be considered. Hexagonal ferrites are considered as promising candidates for EMI shielding materials. This work fabricated Cu, Co, and Ti co-doped $SrFe_{12}O_{19}$ ($SrFe_{12-2x}(Cu_{0.5}Co_{0.5}Ti)_xO_{19}$) samples to investigate EMI shielding properties. Among the samples, the doped ones exhibited better EMI shielding performance than the undoped one, which could be judged through total shielding efficiency ($SE_T$). In addition, the samples exhibited the best shielding performance in the frequency range of 8–12 GHz (X-band), with the best value of $SE_T$ = 4.20 dB for the $x$ = 0.20 sample, which could block ~62% of the incident microwave. The $x$ = 0.05 sample also exhibited similar values with $SE_T$ = 4.17 dB. The enhancement of $SE_T$ values for doped samples compared to the undoped one could be attributed to the increase in conductivity caused by doping. In addition, the enhancement of $SE_T$ could also be attributed to the effects of the magnetic dipoles combined with the electric dipoles of ferrites.

**Keywords-** $SrFe_{12}O_{19}$, Transitional metal, Doping, EMI shielding, Shielding efficiency.

## 1. Introduction
Recently, humans have faced massive electromagnetic (EM) pollution due to the large-scale use of electronic communication devices. EM pollution is created from EM waves due to the charged particles oscillating (Marin et al., 2008; Park et al., 2009; Zeng & Xu, 2010). EM pollution can seriously affect nearby electronic devices and human health, which need a prime concern as shielding. This shielding could be called electromagnetic interference (EMI) shielding, which could be achieved through electrical conductive shielding and/or partially imparting both magnetic permeability and electrical conductivity (Jan et al., 2017; Saboor et al., 2016; Saboor et al., 2018; Saboor et al., 2019). Two mechanisms in EMI shielding, reflection and absorption, prevent incident waves and absorb waves, then generate heat energy

inside the shielding materials, respectively. The total amount of reflected and absorbed energy could be considered total shielding effectiveness. The first candidate for EMI shielding is metals or alloys (Sivaprakash et al., 2023), which still have severe drawbacks, such as corrosion, complicated processing, and high weight. Therefore, more potential candidates should be considered.

Ferrites, including spinel ferrite, garnet, and hexaferrite, could be promising candidates (Oh et al., 2023). Among ferrites, M-type strontium hexaferrite ($SrFe_{12}O_{19}$) has intriguing properties of large magnetization, large magneto-crystalline anisotropy, excellent high-frequency response, and high stability, which could be used in many practical applications such as magnetic recording media, permanent magnets, and microwave absorbers (Chitra et al., 2014; Harris et al., 2009; Luo et al., 2014). Doping on the $SrFe_{12}O_{19}$ host lattice would effectively improve their EMI shielding properties (Lu et al., 2024; Mohammed et al., 2019). This work would investigate the EMI properties of Cu, Co, and Ti co-doped on $SrFe_{12}O_{19}$ samples to determine which concentration would be the best among the dopings. The doping concentration was started at 0, with small increments of doping concentration to achieve the pure phase for as many samples as possible. The sintering temperature was selected as low as possible to achieve samples with small grain sizes.

## 2. Experimental Details

$SrFe_{12-2x}(Cu_{0.5}Co_{0.5}Ti)_xO_{19}$ samples were fabricated from $SrCO_3$, $Fe_2O_3$, CuO, $Co_3O_4$, and $TiO_2$ (purchased from Sigma-Aldrich with high purity) using a combination of ball milling and heat treatment methods. Six samples had concentrations of $x$ = 0, 0.05, 0.10, 0.15, 0.20, and 0.25. The fabrication process details were presented in our previous works (Tho et al., 2022; Xuan et al., 2024). The details of the physical properties of these samples were also investigated in our priority works (Tho et al., 2022; Xuan et al., 2024). In this work, the EMI shielding properties were investigated through S-parameters ($S_{11}$, $S_{21}$, $S_{12}$, and $S_{22}$), which were recorded from a vector network analyzer (VNA, Keysight Model PNA-X N5242A). Before measuring S-parameters, the samples were well mixed with paraffin with a volume ratio of 40:60. Then the mixtures were molded into toroidal shapes with inner and outer diameters of 3.04 and 7.00 mm and a thickness of 3.0 mm.

## 3. Results and Discussion

**Figure 1** shows XRD patterns of $SrFe_{12-2x}(Cu_{0.5}Co_{0.5}Ti)_xO_{19}$ samples with different doping concentrations. Structural properties of $x$ = 0–0.15 samples have been detailed and discussed in our previous reports (Tho et al., 2022; Xuan et al., 2024). Only the $x$ = 0 and $x$ = 0.05 samples exhibited the pure phase of M-type hexaferrite with the space group of $P6_3/mmc$. The $x$ = 0.10 and $x$ = 0.15 samples showed impurity phases of $SrFe_2O_4$ (marked by *) and $\alpha$-$Fe_2O_3$ (denoted by #), besides the main phase of M-type hexaferrite. Consequently, the $x$ = 0.20 and $x$ = 0.25 samples also exhibited the purity phases of $SrFe_2O_4$ and $\alpha$-$Fe_2O_3$, where the percentage of impurity phases was higher than those of the $x$ = 0.10 and 0.15 samples. We believe the samples with high doping concentrations required higher sintering temperatures than those with undoped/low doping concentrations. Thus, the impurity phases occurred in these samples. We also believe the pure phase could be achieved for the samples with high doping concentration at appropriate sintering temperatures. However, the samples were sintered at the same temperature to compare other properties easily.

**Figure 2** shows SEM images of $SrFe_{12-2x}(Cu_{0.5}Co_{0.5}Ti)_xO_{19}$ samples, where the morphological properties were significantly changed by the change in doping concentrations. The samples consisted of polygonal particles that were inhomogeneous in shape and size. With the increase in doping concentration, the particles agglomerated to form larger clusters, increasing the average grain size.

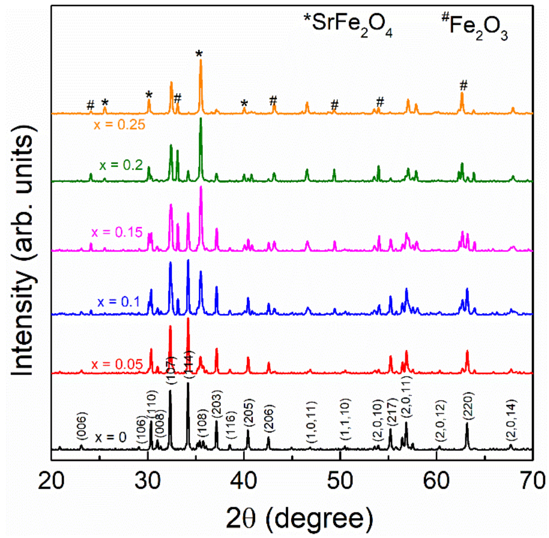


**Figure 1.** XRD patterns of $SrFe_{12-2x}(Cu_{0.5}Co_{0.5}Ti)_xO_{19}$ hexaferrite samples (Tho et al., 2022).

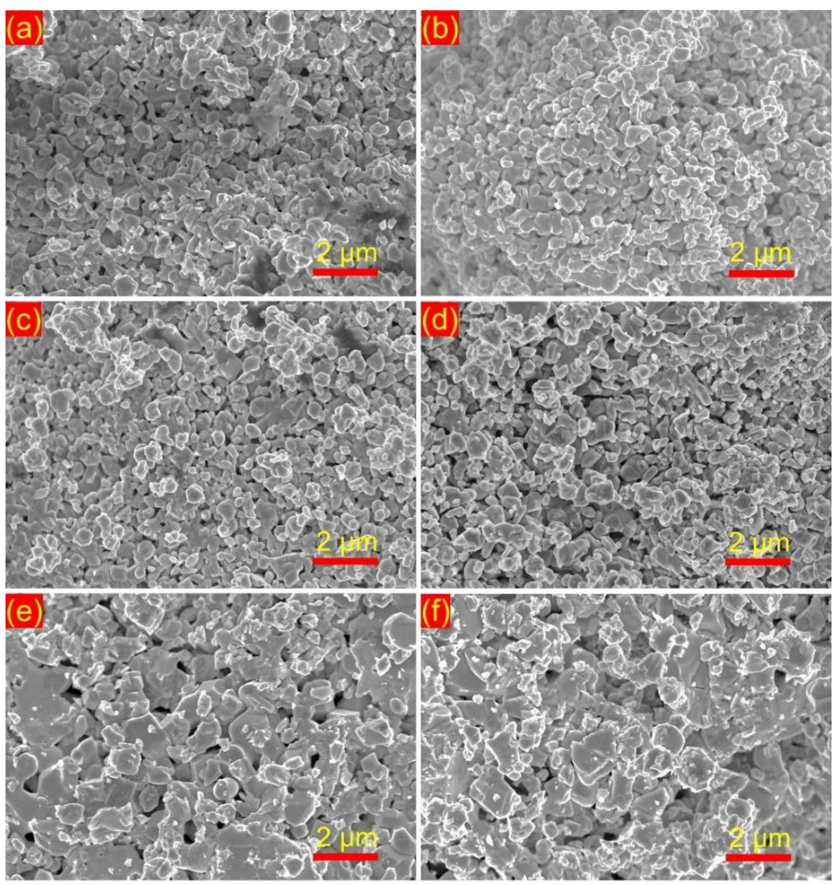


**Figure 2.** SEM images of $SrFe_{12-2x}(Cu_{0.5}Co_{0.5}Ti)_xO_{19}$ hexaferrite samples: (a) $x = 0$, (b) $x = 0.05$, (c) $x = 0.10$, (d) $x = 0.15$, (e) $x = 0.20$, and (f) $x = 0.25$ (Tho et al., 2022; Xuan et al., 2024).

**Figure 3** shows the $S_{11}$ parameter and reflection coefficient curves as a function of frequency. In the $S_{11}$ parameter curves, the $x = 0$ sample had the lowest values in the 2–10 GHz range, and the $x = 0.15$ sample mostly had the lowest values in the 10–18 GHz range (as shown in **Figure 3(a)**). Actually, the $x = 0.25$ sample had some points that showed the lowest $S_{11}$ values in the frequency at 18 GHz. Overall, the $S_{11}$ curves had low values at two ends and high values at the centered frequencies, meaning that the microwave energy was mostly absorbed at two ends and mainly reflected at the centered frequency. From the $S_{11}$ data, the reflection coefficient ($R$) could be calculated through the equation $R = |S_{11}|^2 = |S_{22}|^2$. The $R$ values could be divided into two ranges with opposite tendencies, which were similar to the $S_{11}$ values' tendency. The $R$ values increased with the frequency increase in the 2–10 GHz range, and the $x = 0.25$ sample had the highest $R$-value. Meanwhile, the $R$-value decreased with the frequency increase in the 10–18 GHz range, and the $x = 0.10$ sample had the highest value in this range (as shown in **Figure 3(b)**). The lower R values at the two ends could originate from ferromagnetic resonance frequency ($f_{FMR}$) at these frequencies (Lee et al., 2023). According to the EMI shielding theory, the high $R$-value could result from the sample's high electrical conductivity (Shakir et al., 2022). With the increased doping concentration, the DC conductivity increased in the 2–10 GHz frequency range, thus increasing the reflection coefficient. With the frequency higher than 10 GHz, the DC conductivity decreased, leading to a decrease in $R$ values.

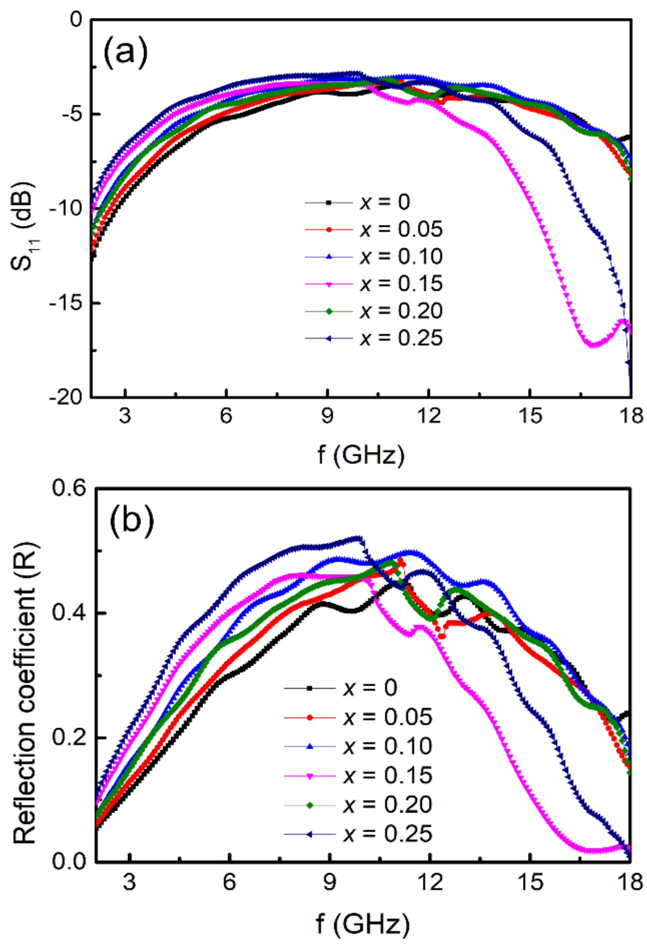


**Figure 3.** Frequency dependence of (a) the $S_{11}$ parameter and (b) the $R$-coefficient of $SrFe_{12-2x}(Cu_{0.5}Co_{0.5}Ti)_xO_{19}$ hexaferrite samples.

**Figure 4** shows the $S_{21}$ parameter and transmission coefficient curves as a function of frequency. In opposite tendencies with the $S_{11}$ parameter, the $S_{21}$ parameter decreased with the increase of frequency in the range of 2–10 GHz and then increased with the increase of frequency in the range of 10–18 GHz (as shown in **Figure 4(a)**). In detail, the $x = 0$ sample mostly showed the highest $S_{21}$ value in the frequency range of 2–10 GHz, and the $x = 0.25$ sample showed the lowest value in this frequency range. In the frequency range of 10–18 GHz, the $x = 0.20$ sample showed the lowest value, and the highest values were achieved for the $x = 0.15$ sample (in the frequency range of 10–16 GHz) and the $x = 0.25$ sample (in the frequency range of 16–18 GHz). The transmission coefficient ($T$) could be calculated from $S_{21}$ values through the equation $T = |S_{21}|^2 = |S_{12}|^2$. The $T$ tendencies of the samples, of course, were similar to those of the $S_{21}$ ones, where $T$ values were highest for the $x = 0$, $x = 0.15$, and $x = 0.25$ samples in the range of 2–10, 10–16, and 16–18 GHz, respectively (as shown in **Figure 4(b)**).

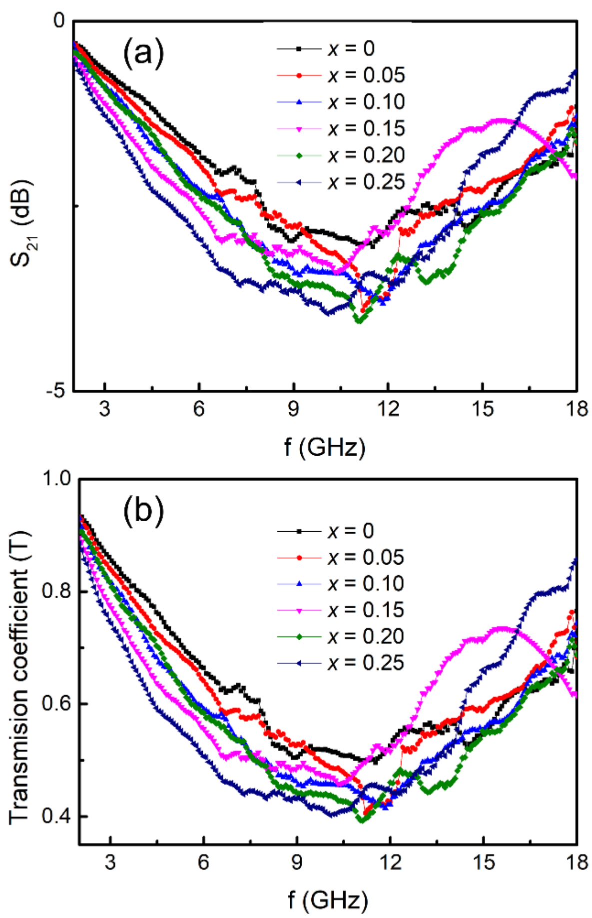


**Figure 4.** Frequency dependence of (a) the $S_{21}$ parameter and (b) the $T$-coefficient of $SrFe_{12-2x}(Cu_{0.5}Co_{0.5}Ti)_xO_{19}$ hexaferrite samples.

After calculating the $R$ and $T$ coefficients, the absorption coefficient ($A$) could be calculated through the equation $A = 1 - R - T$. **Figure 5** shows the $A$-coefficient as a function of frequency, where the $A$ values were mainly below 0.1 in the frequency range of 2–8 GHz and relaxation around 0.1 for the frequency range of 8–18 GHz, except for the $x = 0.15$ sample. The high $A$ values of the $x = 0.15$ sample in the frequency range of 14–18 GHz implied the high absorption capability of the $x = 0.15$ sample in that frequency range.

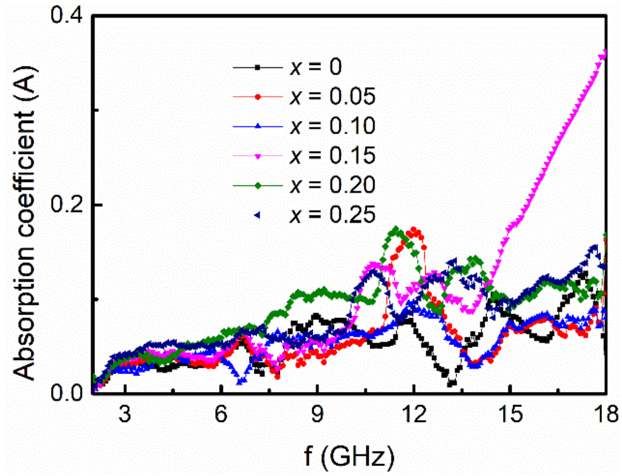


**Figure 5.** Frequency dependence of the *A*-coefficient of $SrFe_{12-2x}(Cu_{0.5}Co_{0.5}Ti)_xO_{19}$ hexaferrite samples.

After calculating the *R* coefficient, the reflection shielding efficiency ($SE_R$) could be calculated through the equation $SE_R = –10 \log(1 – R) = –10 \log(1 – |S_{11}|^2)$ (Khan et al., 2022; Singh et al., 2008). **Figure 6** shows $SE_R$ curves as a function of frequency, which had similar tendencies to the *R*-coefficient. The highest $SE_R$ values could be obtained for the $x = 0.25$ sample, followed by the $x = 0.10$ sample.

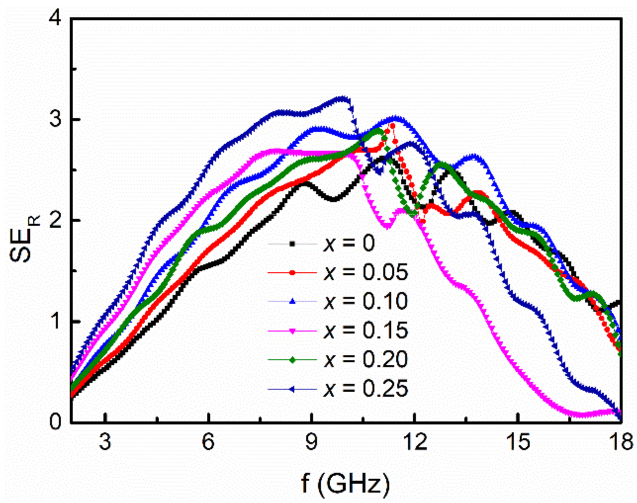


**Figure 6.** Frequency dependence of $SE_R$ of $SrFe_{12-2x}(Cu_{0.5}Co_{0.5}Ti)_xO_{19}$ hexaferrite samples.

Following $SE_R$, the absorption shielding efficiency ($SE_A$) could be calculated through the equation of $SE_A = –10 \log(1 – A_{eff})$, where $A_{eff}$ is the effective absorbance, which could be calculated through *R* and *T* coefficients through the equation of $A_{eff} = (1 – R – T)/(1 – R)$ (Saini et al., 2009). Therefore, the $SE_A$ equation could be rewritten as $SE_A = –10 \log (T/(1 – R))$. The $SE_A$ curves of the samples had similar tendencies with the *A*-coefficient, where the $x = 0.15$ sample had high values in the frequency range of 14–18 GHz, and the $x = 0.20$ sample mostly had high values in the frequency range of 8–14 GHz (as shown in **Figure 7**). The differences in frequency at the highest values of $SE_A$ could be attributed to the presence of impurity phases. As mentioned above, the percentages of $SrFe_2O_4$ and $\alpha$-$Fe_2O_3$ in the $x = 0.20$ sample were higher than those in the $x = 0.15$ samples, leading to a decrease in frequency for maximum $SE_A$ values. Compared to the $SE_R$

values, the $SE_A$ values were much lower, meaning that reflection was the primary shielding mechanism for the shielding effectiveness of the sample. This could also be used to explain the quite noisy data from the $SE_A$.

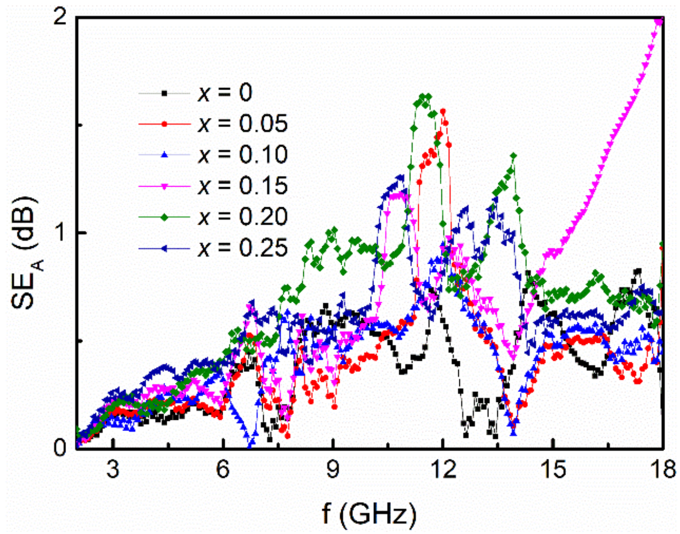


**Figure 7.** Frequency dependence of $SE_A$ of $SrFe_{12-2x}(Cu_{0.5}Co_{0.5}Ti)_xO_{19}$ hexaferrite samples.

**Figure 8(a)** shows total shielding efficiency ($SE_T$) in the 2–18 GHz frequency range, which could be the sum of $SE_R$ and $SE_A$. The detail equation is $SE_T = SE_R + SE_A = -10\log(|S_{21}|^2)$. In overall tendencies, the $SE_T$ values increased with the increase in frequency to about 10 GHz, then decreased when the frequency increased from 10 to 18 GHz. The $SE_T$ increased with doping elements in the 2–10 GHz frequency range among the samples. The difference in $SE_T$ between undoped and doped samples was not visible in the 10–18 GHz frequency range. **Figure 8(b)** shows the enlarged view of **Figure 8(a)** in the X band, which confirms the most stable shielding performance of all samples in this band (8–12 GHz). Among the samples, the shielding performance of doped samples was higher than that of undoped one, where the best performances could be achieved for the $x = 0.05$, 0.20, and 0.25 samples.

In order to clarify the effects of doping on the EMI shielding properties of the $SrFe_{12-2x}(Cu_{0.5}Co_{0.5}Ti)_xO_{19}$, the maximum $SE_T$ values were determined and plotted in **Figure 9**. The $x = 0$ (undoped) sample had a maximum $SE_T$ value of 3.12 dB, the lowest among the samples. With the first doping (the $x = 0.05$ sample), the maximum $SE_T$ value increased to 4.17 dB. Higher doping concentrations decreased the maximum $SE_T$ values to 3.85 and 3.52 dB for the $x = 0.10$ and 0.15 samples, respectively. When the doping concentration reached 0.20, the sample achieved the best maximum $SE_T$ with a value of 4.20 dB, which could be blocked by ~62% of the incident microwave. Then, the maximum $SE_T$ value decreased to 4.01 dB for the $x = 0.25$ sample. It is worth noting that the $SE_T$ value depends on complex permittivity and complex permeability (Gholampoor et al., 2017). In addition, the $SE_T$ of EMI strongly depends on the frequency, the sample's thickness, and the material's conductivity. Thus, the best maximum $SE_T$ values in the $x = 0.05$ and 0.20 samples could be attributed to their highest conductivity caused by doping and the formation and percentages of impurity phases. Furthermore, the enhancement of the $SE_T$ could also be attributed to the synergistic effects of the magnetic dipoles of ferrites and electric dipoles (Kozlovskiy et al., 2021; Shlimas et al., 2021).

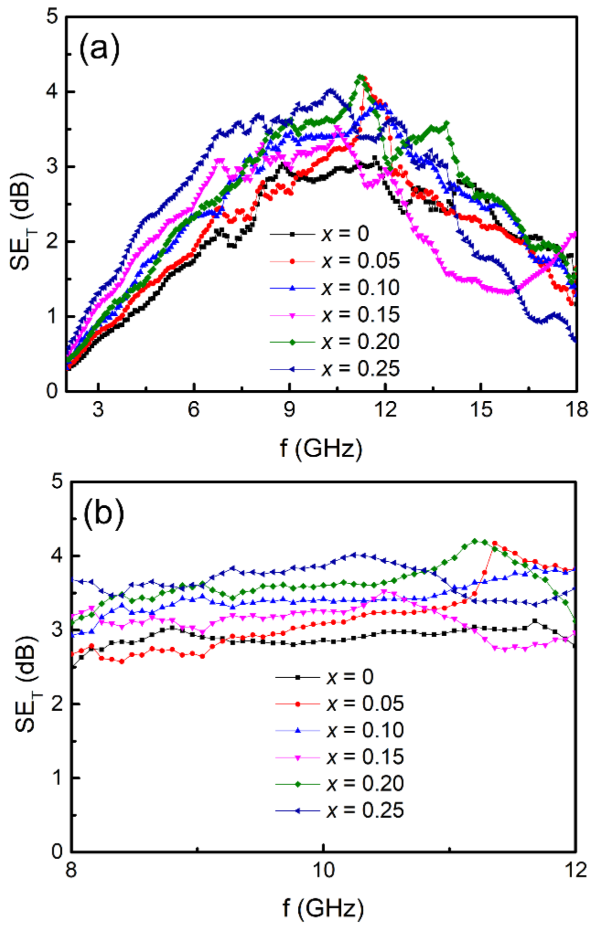


**Figure 8.** Frequency dependence of $SE_T$ of $SrFe_{12-2x}(Cu_{0.5}Co_{0.5}Ti)_xO_{19}$ hexaferrite samples in the frequency ranges (a) 2–18 GHz and (b) 12–18 GHz (enlarged view).

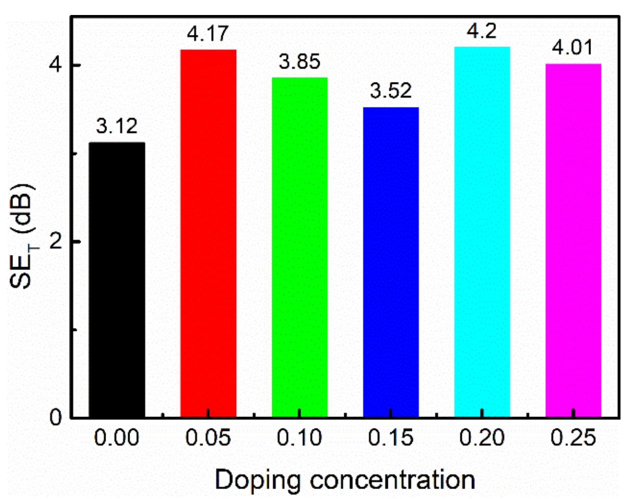


**Figure 9.** Maximum $SE_T$ values for each sample of $SrFe_{12-2x}(Cu_{0.5}Co_{0.5}Ti)_xO_{19}$ hexaferrite.

In order to have a comparison among some related ferrites, their EMI shielding efficiency was listed in **Table 1**. Lu et al. reported (2024) that $Sr_{1-x}Sm_xFe_{12-y}Mn_yO_{19}$ samples reached the best $SE_T$ values with $x$ = 0.075 and $y$ = 0.75, with the $SE_T$ values varying in the range of 0.8–1.6 dB (Lu et al., 2024). These values were much lower than the $SE_T$ values in this work. $Zn_xCu_{(1-x)}Fe_2O_4$ nanoparticles (NPs) prepared by the sol-gel auto-combustion method achieved $SE_T$ values of 4–9 dB (Kavas et al., 2014), which were comparable to our work. In order to achieve higher $SE_T$ values, ferrite should be part of composites, including magnetic and dielectric components. For example, PANI/MWCNTs/$Fe_3O_4$, PANI@$Fe_3O_4$ hybrid, and $Fe_3O_4$@PANI NPs composites achieved $SE_T$ values of 16, 29.3, and 35.1 dB, respectively (Cao et al., 2012; Shukla, 2019; Sun et al., 2013). Similarly, composites of electroless platted FeCo magnetic metal hollow fibers and ethylene propylene diene monomer (EPDM) could reach a $SE_T$ value of 30 dB for a thickness of 3.0 mm (Choi et al., 2015). In this composite, the magnetic alloy of FeCo could benefit EMI shielding effectiveness.

**Table 1.** Comparison of the EMI shielding efficiency of some ferrite materials.

| Sample | Fabrication method | Filler loading (%) | Thickness (mm) | $SE_T$ (dB) | References |
|---|---|---|---|---|---|
| $Zn_xCu_{(1-x)}Fe_2O_4$ NPs | Sol-gel auto combustion | 50% | 3.0 | 4-9 | Kavas et al. (2014) |
| PANI/MWCNTs/$Fe_3O_4$ | Co-precipitation | - | 4.0 | 16 | Cao et al. (2012) |
| FeCo/EPDM | Electroless plating process | - | 3.0 | 30 | Choi et al. (2015) |
| PANI@$Fe_3O_4$ hybrid | Solvothermal | - | 4.5 | 29.3 | Shukla (2019) |
| $Fe_3O_4$@PANI NPs | Oxidation-reduction | - | 1.7 | 35.1 | Sun et al. (2013) |
| $Sr_{1-x}Sm_xFe_{12-y}Mn_yO_{19}$; $x$ = 0.075, $y$ = 0.75 | Sol-gel | 20% | - | ~0.8 | Lu et al. (2024) |
| | | 30% | - | ~1.0 | |
| | | 50% | - | ~1.6 | |
| $SrFe_{12-2x}(Cu_{0.5}Co_{0.5}Ti)_xO_{19}$, $x$ = 0 | Ball milling and heat treatment | 40% | 3.0 | 3.12 | This work |
| $SrFe_{12-2x}(Cu_{0.5}Co_{0.5}Ti)_xO_{19}$, $x$ = 0.05 | | | | 4.17 | |
| $SrFe_{12-2x}(Cu_{0.5}Co_{0.5}Ti)_xO_{19}$, $x$ = 0.10 | | | | 3.85 | |
| $SrFe_{12-2x}(Cu_{0.5}Co_{0.5}Ti)_xO_{19}$, $x$ = 0.15 | | | | 3.52 | |
| $SrFe_{12-2x}(Cu_{0.5}Co_{0.5}Ti)_xO_{19}$, $x$ = 0.20 | | | | 4.20 | |
| $SrFe_{12-2x}(Cu_{0.5}Co_{0.5}Ti)_xO_{19}$, $x$ = 0.25 | | | | 4.01 | |

## 4. Conclusion

This work investigated the EMI shielding properties of $SrFe_{12-2x}(Cu_{0.5}Co_{0.5}Ti)_xO_{19}$ samples through scattering parameters. Reflection shielding efficiency ($SE_R$) mainly contributed to the total shielding efficiency ($SE_T$). The $SE_T$ increased with the frequency increase in the frequency range of 2–10 GHz, then mainly decreased in the frequency range of 10–18 GHz. The maximum $SE_T$ values of all doped samples were higher than that of the undoped one. Among the doped samples, the $x$ = 0.05 and 0.20 samples showed the best $SE_T$ with values of 4.17 and 4.20 dB, respectively. The enhancement of EMI shielding properties of the doped samples could be attributed to the increase in conductivity caused by doping and the combination effects of the magnetic dipoles of ferrites and electric dipoles. The $SE_T$ values of our samples were better or comparable to the $SE_T$ values of M-type hexaferrites and spinel ferrites.

### Conflict of Interest

The authors confirm that there is no conflict of interest to declare for this publication.

### Acknowledgments

The authors express their gratitude for all the valuable support from Duy Tan University, which is going to celebrate its 30th anniversary of establishment (Nov. 11, 1994–Nov. 11, 2024) towards "Integral, Sustainable and Stable Development".

## References

Cao, M.S., Yang, J., Song, W.L., Zhang, D.Q., Wen, B., Jin, H.B., Hou, Z.L., & Yuan, J. (2012). Ferroferric oxide/multiwalled carbon nanotube vs polyaniline/ferroferric oxide/multiwalled carbon nanotube multiheterostructures for highly effective microwave absorption. *ACS Applied Materials & Interfaces*, *4*(12), 6949-6956. https://doi.org/10.1021/am3021069.

Chitra, P., Muthusamy, A., Jayaprakash, R., & Kumar, E.R. (2014). Effect of ultrasonication on particle size and magnetic properties of polyaniline NiCoFe2O4 nanocomposites. *Journal of Magnetism and Magnetic Materials*, *366*, 55-63. https://doi.org/10.1016/j.jmmm.2014.04.024.

Choi, J.R., Jung, B.M., Choi, U.H., Cho, S.C., Park, K.H., Kim, W.J., Lee, S.K., & Lee, S.B. (2015). Characterization of FeCo magnetic metal hollow Fiber/EPDM composites for electromagnetic interference shielding. *Composites Research*, *28*(6), 333-339.

Gholampoor, M., Movassagh-Alanagh, F., & Salimkhani, H. (2017). Fabrication of nano-Fe3O4 3D structure on carbon fibers as a microwave absorber and EMI shielding composite by modified EPD method. *Solid State Sciences*, *64*, 51-61. https://doi.org/10.1016/j.solidstatesciences.2016.12.005.

Harris, V.G., Geiler, A., Chen, Y., Yoon, S.D., Wu, M., Yang, A., Chen, Z., He, P., Parimi, P.V., Zuo, X., Patton, C.E., Abe, M., Acher, O., & Vittoria, C. (2009). Recent advances in processing and applications of microwave ferrites. *Journal of Magnetism and Magnetic Materials*, *321*(14), 2035-2047. https://doi.org/10.1016/j.jmmm.2009.01.004.

Jan, R., Saboor, A., Khan, A.N., & Ahmad, I. (2017). Estimating EMI shielding effectiveness of graphene-polymer composites at elevated temperatures. *Materials Research Express*, *4*(8), 085605. https://doi.org/10.1088/2053-1591/aa81e9.

Kavas, H.Ü.S.E.Y.İ.N., Baykal, A., Demir, A.Y.Ş.E., Toprak, M.S., & Aktaş, B. (2014). Zn x Cu (1− x) Fe 2 O 4 nanoferrites by sol–gel auto combustion route: cation distribution and microwave absorption properties. *Journal of Inorganic and Organometallic Polymers and Materials*, *24*, 963-970. https://doi.org/10.1007/s10904-014-0069-1.

Khan, S.A., Ali, I., Hussain, A., Javed, H.M.A., Turchenko, V.A., Trukhanov, A.V., & Trukhanov, S.V. (2022). Synthesis and characterization of composites with Y-hexaferrites for electromagnetic interference shielding applications. *Magnetochemistry*, *8*(12), 186. https://doi.org/10.3390/magnetochemistry8120186.

Kozlovskiy, A.L., Shlimas, D.I., & Zdorovets, M.V. (2021). Synthesis, structural properties and shielding efficiency of glasses based on TeO 2-(1-x) ZnO-xSm 2 O 3. *Journal of Materials Science: Materials in Electronics*, *32*, 12111-12120. https://doi.org/10.1007/s10854-021-05839-0.

Lee, H., Ryu, S.H., Kwon, S.J., Choi, J.R., Lee, S.B., & Park, B. (2023). Absorption-dominant mmWave EMI shielding films with ultralow reflection using ferromagnetic resonance frequency tunable M-type ferrites. *Nano-Micro Letters*, *15*(1), 76. https://doi.org/10.1007/s40820-023-01058-w.

Lu, Y., Akhtar, M.N., Yousaf, M., Katubi, K.M., Irfan, M., Khan, M.A., Mahmoud, M., Almohammedi, A., Ullah, S., Alrowaili, Z.A., & Al-Buriahi, M.S. (2024). Structural, morphological, and EMI shielding evaluations of Sm-Mn co-doped Sr-based M-type hexaferrite for Ku band applications. *Journal of Alloys and Compounds*, *994*, 174627. https://doi.org/10.1016/j.jallcom.2024.174627.

Luo, J., Xu, Y., & Gao, D. (2014). Synthesis, characterization and microwave absorption properties of polyaniline/Sm-doped strontium ferrite nanocomposite. *Solid State Sciences*, *37*, 40-46. https://doi.org/10.1016/j.solidstatesciences.2014.08.007.

Marin, P., Cortina, D., & Hernando, A. (2008). Electromagnetic wave absorbing material based on magnetic microwires. *IEEE Transactions on Magnetics*, *44*(11), 3934-3937. https://doi.org/10.1109/TMAG.2008.2002472.

Mohammed, J., Trudel, T.T.C., Hafeez, H.Y., Basandrai, D., Bhadu, G.R., Godara, S.K., Narang, S.B., & Srivastava, A.K. (2019). Design of nano-sized Pr 3+–Co 2+-substituted M-type strontium hexaferrites for optical sensing and electromagnetic interference (EMI) shielding in K u band. *Applied Physics A*, *125*, 251. https://doi.org/10.1007/s00339-019-2545-5.

Oh, W., Hajra, S., Divya, S., Panda, S., Oh, Y., Jaglic, Z., Pakawanit, P., Oh, T.H., & Kim, H.J. (2023). Contact electrification of porous PDMS-nickel ferrite composites for effective energy harvesting. *Materials Science and Engineering: B*, *292*, 116397. https://doi.org/10.1016/j.mseb.2023.116397.

Park, K.Y., Han, J.H., Lee, S.B., Kim, J.B., Yi, J.W., & Lee, S.K. (2009). Fabrication and electromagnetic characteristics of microwave absorbers containing carbon nanofibers and NiFe particles. *Composites Science and Technology*, *69*(7-8), 1271-1278. https://doi.org/10.1016/j.compscitech.2009.02.033.

Saboor, A., Khalid, S.M., Jan, R., Khan, A.N., Zia, T., Farooq, M.U., Afridi, S., Sadiq, M., & Arif, M. (2019). PS/PANI/MoS2 hybrid polymer composites with high dielectric behavior and electrical conductivity for EMI shielding effectiveness. *Materials*, *12*(17), 2690. https://doi.org/10.3390/ma12172690.

Saboor, A., Khan, A.N., Cheema, H.M., Yaqoob, K., & Shafqat, A. (2016). Effect of polyaniline on the dielectric and EMI shielding behaviors of styrene acrylonitrile. *Journal of Materials Science: Materials in Electronics*, *27*, 9634-9641. https://doi.org/10.1007/s10854-016-5021-4.

Saboor, A., Khan, A.N., Jan, R., Sharif, S., & Khan, M. (2018). Mechanical, dielectric and EMI shielding response of styrene acrylonitrile, styrene acrylonitrile/polyaniline polymer blends, upon incorporation of few layer graphene at low filler loadings. *Journal of Polymer Research*, *25*, 248. https://doi.org/10.1007/s10965-018-1648-6.

Saini, P., Choudhary, V., Singh, B.P., Mathur, R.B., & Dhawan, S.K. (2009). Polyaniline–MWCNT nanocomposites for microwave absorption and EMI shielding. *Materials Chemistry and Physics*, *113*(2-3), 919-926. https://doi.org/10.1016/j.matchemphys.2008.08.065.

Shakir, H.F., Shahzad, M., Aziz, H.R., Rizwan, M.S., Shahid, S., Ali, S.H., & Zhao, T. (2022). In-situ polymerization and EMI shielding property of barium hexaferrite/pyrrole nanocomposite. *Journal of Alloys and Compounds*, *902*, 163847. https://doi.org/10.1016/j.jallcom.2022.163847.

Shlimas, D.I., Kozlovskiy, A.L., & Zdorovets, M.V. (2021). Study of the formation effect of the cubic phase of LiTiO2 on the structural, optical, and mechanical properties of Li2±x Ti1±x O3 ceramics with different contents of the X component. *Journal of Materials Science: Materials in Electronics*, *32*(6), 7410-7422. https://doi.org/10.1007/s10854-021-05454-z.

Shukla, V. (2019). Review of electromagnetic interference shielding materials fabricated by iron ingredients. *Nanoscale Advances*, *1*(5), 1640-1671. https://doi.org/10.1039/C9NA00108E.

Singh, K., Ohlan, A., Saini, P., & Dhawan, S.K. (2008). Poly (3, 4-ethylenedioxythiophene) γ-Fe2O3 polymer composite–super paramagnetic behavior and variable range hopping 1D conduction mechanism–synthesis and characterization. *Polymers for Advanced Technologies*, *19*(3), 229-236.

Sivaprakash, P., Kim, I., Divya, S., Hajra, S., Oh, T.H., & Muthu, S.E. (2023). Influence of non-magnetic Cu on structural, magnetic and magnetocaloric properties on NiMnIn bulk Heusler alloys. *Materials Science and Engineering: B*, *297*, 116760. https://doi.org/10.1016/j.mseb.2023.116760.

Sun, Y., Liu, X., Jin, C., Xia, A., Zhao, S., Li, W., Feng, C., Xiao, F., & Wu, Y. (2013). A facile route to carbon-coated vanadium carbide nanocapsules as microwave absorbers. *RSC Advance*. *3*, 18082-18086. https://doi.org/10.1039/C3RA42544D.

Tho, P.T., Xuan, C.T. A., Tran, N., Tuan, N.Q., Jeong, W.H., Kim, S.W., Dat, T.Q., Nguyen, V.D., Bach, T.N., Thanh, T.D., Khan, D.T., & Lee, B.W. (2022). Ultra-wide effective absorption bandwidth of Cu, Co, and Ti co-doped SrFe12O19 hexaferrite. *Ceramics International*, *48*(19), 27409-27419. https://doi.org/10.1016/j.ceramint.2022.05.389.

Xuan, C.T.A., Toan, H.N., Ha, P.T.V., Ho, T.A., Thanh, T.D., Tuan, N.Q., Tho, P.T., & Tran, N. (2024). Microwave absorption performance for Cu, Co, and Ti co-doped SrFe12O19 as a function of incident angle. *Materials Chemistry and Physics*, *317*, 129174. https://doi.org/10.1016/j.matchemphys.2024.129174.

Zeng, J., & Xu, J. (2010). Microwave absorption properties of CuO/Co/carbon fiber composites synthesized by thermal oxidation. *Journal of Alloys and Compounds*, *493*(1-2), L39-L41. https://doi.org/10.1016/j.jallcom.2009.12.192.